In-situ quantification of manufacturing-induced strains in fiber metal laminates with strain gages

Johannes Wiedemann[a,*], Robert Prussak[b], Erik Kappel[b] and Christian Hühne[a,b]

[a]*TU Braunschweig, Institute of Mechanics and Adaptronics, Langer Kamp 6, Braunschweig, 38100, Germany*
[b]*DLR, Institute of Composite Structures and Adaptive Systems, Lilienthalplatz 7, Braunschweig, 38108, Germany*

ABSTRACT

The predominant use of FBG sensors to characterize the residual stress state in composite materials to date does not permit absolute strain measurements. The reason for this is the loss of the connection between the sensor and laminate during phase transitions of the resin. Thus, points of significant changes in the measurement signal (e.g. bonding temperature) need to be used for the residual stress evaluation. For fiber metal laminates (FML) however, strain gages applied to the metal layer allow absolute strain measurements since the metal behaves purely elastic over the entire manufacturing process. Hence, residual stresses in the metal layer of an FML are quantified directly. Despite the sensors being applied to the metal layer, it is shown that the cure state of the resin can still be analyzed by changes in the coefficient of thermal expansion. Thus, the effects of different modifications to the cure cycle are assessed in terms of residual stress reduction. It is shown that assuming the bonding temperature to be equal to the stress-free temperature results in a conservative estimation of the residual stress state. The strain gage signal is shown to be in good agreement with FBG sensor data during a combined experiment.

1. Introduction

The knowledge of the manufacturing-induced residual stress state in a composite structure is of great interest since residual stresses influence the mechanical properties and lead to geometric deviations of a manufactured part, up to failure at unexpected load levels. This applies for all composite materials and is predominantly influenced by the differences in the thermal expansion behavior of the individual components combined with elevated temperatures during manufacturing. For epoxy based resin systems this is accompanied by the chemical shrinkage of the resin during cure. For fiber metal laminates (FML) the thermal incompatibility is particularly relevant since the constituents – metal and fiber-reinforced polymer (FRP) – show very different coefficients of thermal expansion (CTEs) and need to be cured at temperatures up to 180 °C. [1]

FMLs are a group of materials that consist of alternating layers of thin metal and FRP plies intending to get a superior material by combining the advantages of the two basic components. The best-known representative of this group of materials is GLARE, a laminate with alternating glass fiber reinforced epoxy and aluminum layers. GLARE is used in industry e.g. by AIRBUS for large-scale fuselage panels in the long-range aircraft A380. [2]

Another potential FML candidate is the combination of carbon fiber reinforced polymer (CFRP) with steel or titanium. Based on the relevant literature, this group of FML can be divided into two main application scenarios as Table 1 shows. On the one hand, CFRP-steel laminates are used as

Table 1
Overview of CFRP-steel/titanium applications distinguished by global and local application scenarios

CFRP-steel/titanium as structural material	
- Dominantly UD loaded structures	[3–5]
- Function integration	[6–8]
- Crash structures	[9]
CFRP-steel/titanium for local property enhancement	
- Bearing strength	[10–13]
- Erosion	[14, 15]

a structural material for selected load cases. On the other hand, CFRP-steel laminates were extensively investigated for local property enhancement of CFRP parts. However, no matter what the application scenario or the material combination is, residual stresses arise inevitably during the manufacturing process. In this work, the focus is on CFRP-steel laminates, but the results are easily transferred to any other FML variant.

Since stresses can not be directly measured, the question arises as to how a residual stress state can be quantified in an FML component. The exact quantification is especially important when the influence of the inherent stresses on other relevant parameters, as for example compression after impact (CAI) properties, is of interest. In the context of this work, for example, the influence of the residual stress level on the propagation of guided ultrasonic waves (GUW) is to be known. Thus, a structural health monitoring system based on GUW can consider the influence and distinguish more easily between state characteristic-related detuning and damage-related features [16].

*Corresponding author

✉ johannes.wiedemann@tu-braunschweig.de (J. Wiedemann)

ORCID(s): 0000-0003-2040-0143 (J. Wiedemann); 0000-0002-9777-0495 (R. Prussak); 0000-0002-8760-8451 (E. Kappel); 0000-0002-2218-1223 (C. Hühne)

All measuring methods to determine residual stresses monitor strains or measure deformations of composite parts, from where the resulting stresses are calculated. The most common techniques presented in literature mainly differ in their time of application regarding the manufacturing process. During manufacturing mainly embedded sensors (e.g. fiber Bragg gratings (FBGs) or strain gages (SGs)) are used, whereas, after manufacturing, there are several non-destructive (e.g. curvature measurement) and destructive methods (e.g. layer removal). [17]

There is an advantage in considering FMLs in the context of manufacturing-induced strain analysis. The metal constituent in an FML behaves purely linear elastic during the entire manufacturing process. Thus, when measuring the strains in the metal layer over the entire cure cycle, the residual stresses after manufacturing can directly be quantified. This allows absolute strain measurements with a fixed stress and strain-free zero point at the beginning of the manufacturing process. For composite materials, however, this is challenging, as the load carrying bond between the sensor and base material is only established during the manufacturing process itself [18, 19]. Hence, the recorded strain data can only be interpreted from the point where a firm connection has been developed. Therefore, in this work, the metal layer is instrumented with strain gages in addition to the FBG sensors in the CFRP layers, such that the manufacturing induced strains can be directly quantified during the entire curing process.

To validate the measuring technique, FML specimens with different residual stress levels are manufactured. There are several approaches on how to manipulate the residual stresses in a composite laminate, that range from clamping devices, relaxation techniques after manufacturing to modified cure cycles. The latter have shown to be a powerful and easy to adapt tool to alter the residual stress state in an FML laminate by adjusting the temperature profile during cure. This is known as modified or smart curing in the literature. [19, 20]

Different modified cure cycles (MOD) are compared to the standard manufacturer recommended cure cycle (MRCC) and the recorded strain data and its significant behavior is discussed and interpreted. Subsequently, the resulting residual stress levels are calculated and compared to analytical calculations using the classical laminate theory (CLT).

2. Methods

In this section, the materials used in this work as well as their behavior during manufacturing is presented. Furthermore, the modified cure cycles as applied here are introduced. The focus in this section, however, will be on the origin and the development of the residual stress state as well as on the measurement and calculation of it.

2.1. Materials

The FML laminates in this paper are manufactured from carbon fiber reinforced epoxy prepreg (Hexply 8552-AS4) from the Hexcel company and a high-strength stainless steel

Table 2

Material properties for the single constituents of the CFRP-steel laminates used in this work

	Hexcel 8552-AS4	Steel 1.4310	
E_1	132 [21]	179[a] [22]	GPa
E_2	9.2 [21]	179[b] [22]	GPa
G_{12}	4.8 [21]	71.2 [18]	GPa
ν_{12}	0.3 [21]	0.3 [18]	-
σ_1	2.1 [21]	1.3 [22]	GPa
t_{ply}	0.13[c] [23]	0.12	mm

[a] direction of rolling (DOR), [b] transverse to DOR, [c] cured

alloy (1.4310). Table 2 contains the relevant mechanical material properties.

Besides the mechanical properties for the two materials, the coefficients of thermal expansion (CTEs) are measured using the strain gage technique as it was presented in [24]. Strain gages are applied to the single materials in both the in-plane directions with high-temperature resistant adhesive (TML NP-50B) [25]. During a subsequent heating and cooling cycle, the resulting free thermal strains are recorded. From the recorded strain data, the CTE for the substrate is linearly interpolated. Table 3 shows the results.

The measured CTEs of the single materials $\{\alpha\}_k$ can be used to calculate the thermal expansion coefficients for an arbitrary laminate $\{\alpha\}_{lam}$ by the classical laminate theory [26]. The relevant relation is consistent with [27] and given in Equation 1:

$$\{\alpha\}_{lam} = [R]^{-1} \cdot [A]^{-1} \cdot \sum_{k=1}^{n} \left[\overline{Q}\right]_k \cdot [R] \cdot [T]_k^{-1} \cdot t_k \cdot \{\alpha\}_k \quad (1)$$

$$\text{with } [R] = \begin{bmatrix} 1 & 0 & 0 \\ 0 & 1 & 0 \\ 0 & 0 & 2 \end{bmatrix} \text{ and } [T] = \begin{bmatrix} c^2 & s^2 & 2sc \\ s^2 & c^2 & -2sc \\ -sc & sc & c^2 - s^2 \end{bmatrix}$$

where $[A]$ is the laminate extensional stiffness matrix, $\left[\overline{Q}\right]_k$ the ply stiffness in global laminate coordinates, $[T]$ the transformation matrix and t_k the thickness for each ply respectively. In the transformation matrix, s and c indicate the $sin(\alpha)$ and $cos(\alpha)$ terms, where α is the ply angle in the laminate coordinate system. For further information about the CLT, the reader is refered to [26, 28].

For the specimens used throughout the investigations in this work, a symmetric layup with 4 steel and 12 prepreg plies is used: $[St/0_4/St/0_2]_S$. With this laminate, a metal volume fraction MVF of 24 % is achieved. The calculated CTEs for the laminate are given in Table 3. The calculated values are used for comparison with measured values in the results section.

2.2. Resin kinetics

A thermoset resin passes different phases during cure where the state characteristics influence a measured strain signal. These phases can be ideally illustrated by the development of the degree of cure (DoC) and the glass transition

Table 3

Coefficients of thermal expansion for the FML constituents used in this work. CTEs for the single materials were derived between 55 °C and 95 °C from experiment. Laminate CTEs were calculated with CLT (Equation 1). 0° specifies the fiber direction or the direction of rolling respectively.

Material	0°	90°
Steel 1.4310	19.0 ppm/K	19.15 ppm/K
Hexply 8552-AS4	2.51 ppm/K	33.1 ppm/K
FML $[St/0_4/St/0_2]_S$	7.38 ppm/K	23.84 ppm/K

temperature T_g. The development of these two parameters during the recommended cure cycle for the 8552 resin is shown in Figure 1 over the time of the curing process. The time and temperature-dependent values for DoC and T_g were calculated using a material model developed by [29]. This model follows the CHILE (cure hardening instantaneous linear elastic) approach where the the behavior of the resin is assumed to be linear elastic during a single time increment but the input values are continuously updated before each new increment calculation. This model can accurately describe the material state for rather simple cure cycles without any intermediate cooling steps. Thus, it gives a good representation for the 8552 resin during the MRCC that consists of a two-step temperature profile with a dwell stage at 110 °C and the final cure temperature at 180 °C (see Figure 1).

Two prominent points are marked in the figure that deviate the three phases (A: viscous, B: visco-elastic, C: elastic) from each other. One is defined as the transition from the viscous to the visco-elastic state at a degree of cure of about 55%: Gelation (A → B). If the polymer continues to cure, the glass transition temperature will eventually exceed the process or component temperature. At this point, the polymer changes into a glassy state, in which it behaves predominantly elastically: Vitrification (B → C). [29]

In the first phase, when the polymer is in its viscous state A, it is assumed that no stresses can be transferred between the single layers of the laminate since any load on the resin will be immediately relieved through flow. In the visco-elastic state B, stresses start to build up but can be relieved to some extent over time. Whereas in the elastic state C, the resin behavior is purely linear elastic. Therefore, to reduce the residual stresses in a laminate it is desirable to shift the point of gelation to a temperature as close as possible to room or operating temperature. [17, 19]

2.3. Layup and manufacturing

In the production of FML, the interface between metal and FRP plays a crucial role. The metal layers must be pretreated accordingly so that the interlaminar shear forces between the individual plies of the laminate can be transferred. For the pairing of CFRP with steel, a mechanical pretreatment process with the subsequent application of an aqueous sol-gel solution leads to high interlaminar strengths. [3, 30]
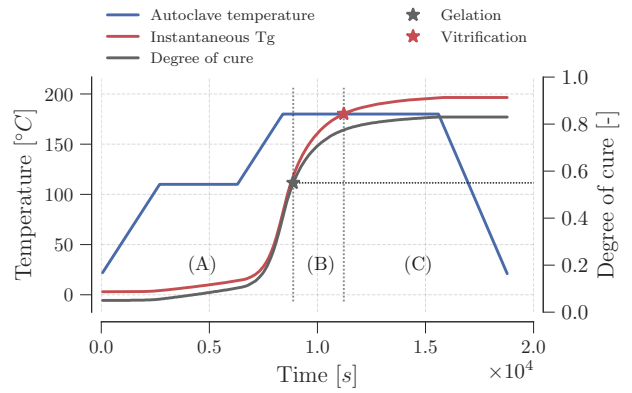

Figure 1: Development of degree of cure and glass transition temperature over time for the manufacturer recommended cure cycle of the 8552 resin. A: viscous state, B: visco-elastic state, C: elastic state
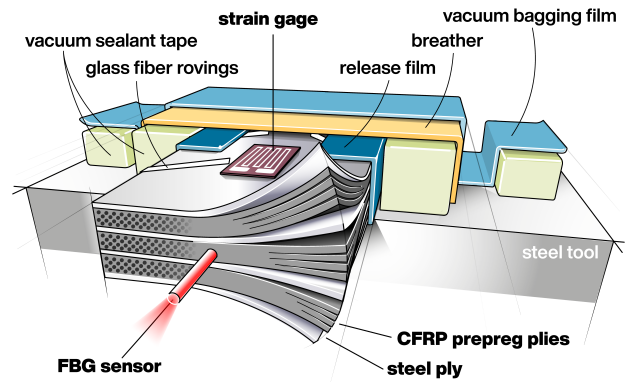

Figure 2: Schematic specimen layup and experimental setup with sensor positions and vacuum bagging

The mechanical pretreatment is carried out with a vacuum suction blasting process, which is beneficial for thin metal layers where a classical sandblasting process would severely damage the foils. After the mechanical treatment, the foils are chemically cleaned with heptane. For the sol-gel treatment, 3M Surface Pre-Treatment AC-130-2 [31] is applied with a brush and then dried for one hour. Subsequently, the foils are stored in a vacuum or laminated immediately.

For the specimens manufactured in this work, the FML-laminates are wrapped in a thin release film with glass fiber rovings placed around the edges to ensure the degassing of the laminate. Subsequently, the uncured laminate is placed on a stainless steel tool on which vacuum sealant tape is used as a border around the laminate. The schematic manufacturing setup is illustrated in Figure 2. The specimens in this work are subsequently cured under a vacuum bag in a laboratory oven to reduce the complexity of the experimental setup. Compared to conventional manufacturing processes in an autoclave, no additional hydrostatic pressure is used during cure.

2.4. Smart cure cycles

There are two main motivations for using smart cure cycles. One is the reduction of process time in an autoclave, by splitting the cure cycle into two steps with the composite part being moved into a curing oven after the gel point has been passed. The second is the reduction of the manufacturing-process-related residual stresses which is the focus in this work. For composites [32, 33] as well as FML [19, 20] the applicability of process modifications to reduce residual stresses was shown. The reduction of the residual stress level comes along with an improvement of the tensile and inter-laminar shear strength of a component, which is beneficial in the context of high performance structures [20, 34].

With smart cure cycles, the temperature at which the resin passes the point of gelation can be changed. The goal is to move this temperature as close as possible to room or operating temperature. This reduces the essential temperature range, which in consequence leads to a reduction of temperature-induced residual stresses as the individual layers of the laminate hinder their free thermal expansion from the time of gelation. In Section 2.5 this is discussed in more detail.

The modification parameter that has the biggest effect on the residual stress level is an intermediate cooling step during the cure cycle [19]. Figure 3 compares the standard MRCC, which was also used for the cure kinetics analysis, to a modified cure cycle that was developed in [19]. The modifications start from the end of the dwell stage, where the heating ramp is altered. After reaching a temperature T_c a cooling step is initiated. The goal is to get the curing reaction in the resin started before cooling the laminate. The chemical curing reaction responds to a temperature change with a certain time lag and is not completely stopped by a temperature drop once initiated. Thus, it can be achieved that the laminate is at a lower temperature in stage II or III of the cure cycle (compare Figure 3) when passing the gel point. After the intermediate cooling step in the MOD cycle, the laminate is slowly heated to the final curing temperature as used in the MRCC to ensure the same degree of cure at the end of the cure cycle.

2.5. Residual stresses

Residual stresses generally occur whenever free strains are hindered by external boundary conditions. In contrast, mechanical stresses are caused by external forces and loads. Consequently, in a homogeneous body that is freely supported, no residual stresses can arise due to e.g. an increase in temperature, since the body can expand freely in all spatial directions without this expansion being impeded. In materials such as FML, however, the single composite constituents have different expansion properties and eventually interact with each other so that residual stresses inevitably arise as a consequence of the manufacturing process. Not only the properties of the constituents but also the process conditions (e.g. tool-part interaction, uneven temperature distribution, vacuum bagging) can influence the residual stress state. However, the thermal incompatibility of the materials used
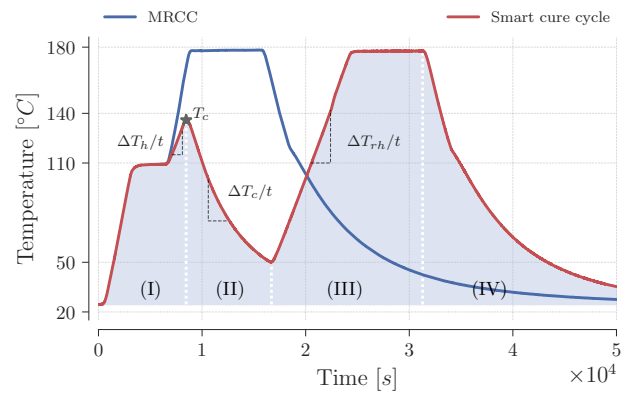

Figure 3: Standard cure cycle compared to typical smart cure cycles with its relevant stages: (I) initial heating with dwell stage, (II) intermediate cooling, (III) re-heating and (IV) final cooling. The heating rate $\Delta T_h/t$ specifies the heating rate starting at the end of the dwell stage.

in FML has the greatest influence on the residual stress state. [11, 17]

When assuming purely linear thermo-elastic behavior, the residual stress state σ_{res} in a laminate can be calculated for each ply k with the CLT. As the laminate in this work only consists of unidirectional CFRP plies, the global laminate CTEs do not need to be transformed into local ply coordinates, which simplifies the relation to:

$$\{\sigma_{res}\}_k = [Q]_k \cdot \left(\left(\{\alpha\}_{lam} - \{\alpha\}_k \right) \cdot \left(T_R - T_{sf} \right) \right) \quad (2)$$

with the reduced stiffness matrix $[Q]_k$ and the coefficients of thermal expansion $\{\alpha\}_k$ for each ply k as well as for the entire laminate $\{\alpha\}_{lam}$. Furthermore, T_R indicates the temperature of interest, e.g. room temperature, and T_{sf} the stress-free temperature. The latter describes the temperature at which a laminate is in its stress-free state and is therefore defined as the stress-free temperature in the literature [35, 36].

However, the CLT does not consider non-linear effects and a critical step in the calculation is the determination of the stress-free temperature. T_{sf} can be determined in various ways. The literature describes experimental methods e.g. with FBGs [18], a combination of FBGs with strain gages [24], using asymmetric layups and curvature evaluation [19] or asymmetric specimens and a consequent heating cycle [18]. Furthermore, the stress-free temperature can be approximately derived from the cure temperature or the glass transition temperature of the material [11, 28].

The literature shows, that depending on the method used, the assumed stress-free temperature can deviate by as much as 40 K [11, 28]. In consequence, the results of the calculated residual stresses for a laminate are directly affected. This emphasizes the need for absolute measurements of the residual stress state in FML, where there is no need of T_{sf} for the calculation of the residual stresses.
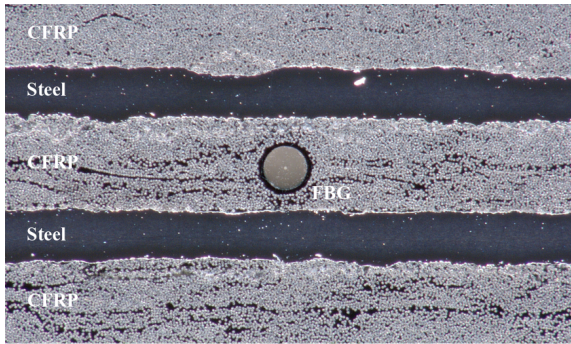
Figure 4: Microsection of a fiber Bragg grating sensor embedded between two CFRP plies in a CFRP-steel laminate

Figure 5: Temperature over time for the three different cure cycles used in this work

2.6. Measurement of curing strains

The most common technique to measure strains evolving during the manufacturing process of fiber composite materials is the use of integrated sensors. Mainly fiber optic sensors (FOS) with Bragg gratings (FBG) (e.g. [37, 38]) are used. This type of sensor has the shape of a single glass fiber with a protective coating around it and can be embedded directly into the FRP without disturbing the laminate on a macro level (see Figure 4). During the curing of the resin, the FOS binds to the matrix and, after binding, experiences strains in the same way as the material around it. However, because the bonding only develops during cure, it is not possible to measure absolute strains in a laminate from the beginning of the manufacturing process. Others, e.g. [39, 40], also use strain gages (SGs), that are placed inside the laminate before cure, but the same problem arises as with the FBG sensors in terms of absolute measurements. Furthermore, an embedded strain gage is a larger discontinuity than an FBG sensor. Wisnom et al. [41] used a spot curing technique to be able to measure strains from the beginning of the manufacturing process. Twigg et al. [42] used SGs on the tool surface to monitor the interaction between a laminate and the metal tool. However, this only provides information about the stress transfer between the laminate and the tool surface, but not about the residual stress state in the laminate itself.

Since the metal component in an FML behaves purely elastic, an instrumented metal layer can be used to record absolute strains starting from the beginning of the curing process. Strain gages are a state-of-the-art technique to monitor strains in metal materials and have already been shown by the authors to be applicable for FML as well [43]. Therefore, the focus of the residual strain measurements is on the strain gage technique in this paper. However, FBG sensors are used to validate the strain signals and to analyze the resin behavior during cure.

The strain gage measurement method that is used in this work was previously described in detail in [43]. The $120\,\Omega$ SG (HBM LC11-6/120) bonded to the metal layer forms one resistance in the Wheatstone-bridge circuit (quarter-bridge arrangement) and is set up in a three-wire hook-up to compensate for any disturbances in the wires themselves. To
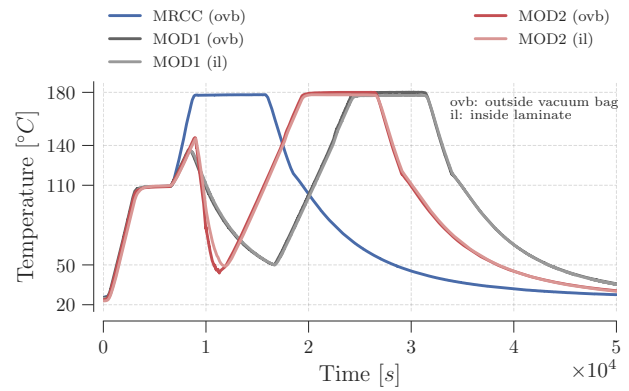
account for the temperature-induced effects, a dummy strain gage is attached to an ultra-low expansion glass specimen and placed on top of the vacuum bag in the oven during experiments. Thus, any thermal strains arising from the strain gage itself are compensated.

With the recorded in-plane strains ε_{res} during cure in the metal component of the FML, the resulting residual stresses σ_{res} in the metal layer can be calculated by applying Hooke's law using the reduced stiffness matrix $[Q]_k$ for the respective ply:

$$\{\sigma_{res}\}_k = [Q]_k \cdot \{\varepsilon_{res}\}_k \qquad (3)$$

The FBG technique was extensively discussed in [18]. A 1550 nm fiber Bragg grating sensor is used in the experiments of this work and the consequent Bragg wavelength shift $\Delta\lambda_b/\lambda_b$ is evaluated. Since the FBG-signal is only used qualitatively to validate the strain gage data (see Section 3.6) no temperature compensation of the signal is performed.

For more details of the measurement techniques, the reader is referred to the two respective publications.

3. Results

The strains developing during several different cure cycles have been recorded with strain gages. In this section, the differences in the cure cycles will be explained which is followed by the strain data analysis. Finally, the residual strains are used to calculate the residual stress state in the metal layer of the laminate, which is validated by CLT calculations and FBG measurements.

3.1. Cure cycles

Different smart cure cycles are used in this work to demonstrate the principle of the in-situ strain gage measurement technique and to discuss the implications for the residual stress state of FML. The cure cycles only differ from each other in the temperature profile over time. The different cure cycles are plotted in Figure 5. The modified cure cycles (MOD) show lower heating rates ($\Delta T_h/t \approx$

(a) Strains in 0°- and 90°-direction for MOD1

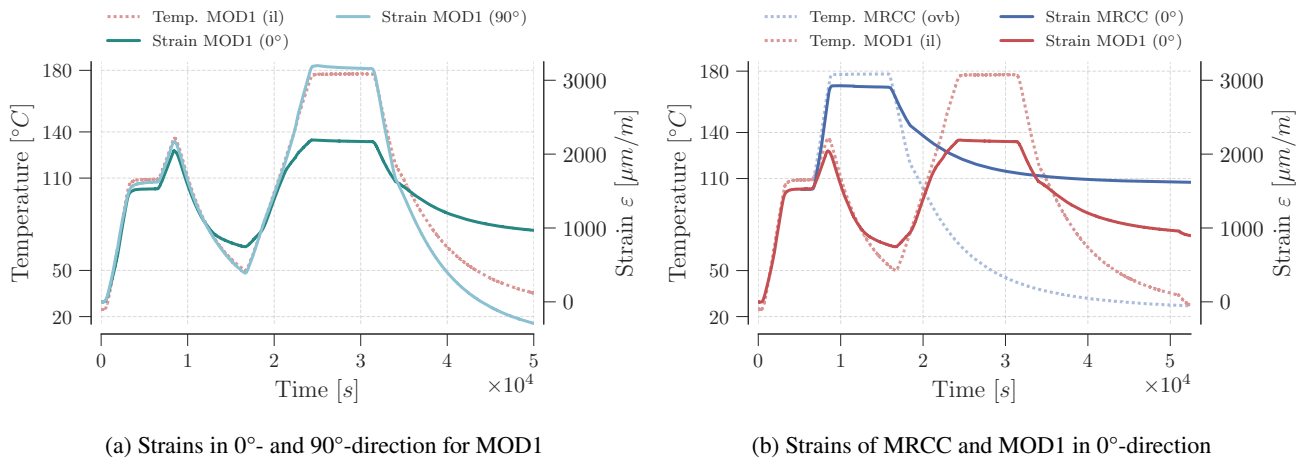(b) Strains of MRCC and MOD1 in 0°-direction

Figure 6: Comparison of measured strain data over time for the two principal in plane orthotropic axes (0° and 90°) for the modified cure cycle MOD1 as well as comparison of the strain signal in 0°-direction to the MRCC

Table 4

Approximate (linearly interpolated) heating and cooling rates as well as maximum temperature T_c before the cooling step is initiated for the different cure cycles in this work in [°C] and [K/min] respectively

Cure cycle	$\Delta T_h/t$	T_c	$\Delta T_c/t$	$\Delta T_{rh}/t$
MRCC	2 (1.9)	-	-	-
MOD1	1 (0.9)	135 (136)	-0.6	1
MOD2	1 (0.9)	145 (146)	-2.3	1

1 °C/min) for the heating ramp after the dwell stage compared to the manufacturer recommended cure cycle (MRCC) ($\Delta T_h/t \approx 2$ °C/min). The MOD cure cycles themselves differ in the maximum temperature (T_c) before the cooling stage is initiated, as well as in the cooling rate ($\Delta T_c/t$).

The rates and temperatures for all the cure cycles are listed in Table 4. For some cure cycles, the temperature was measured with a thermocouple (type K) inside the laminate (il), whereas other temperature measurements were taken outside the vacuum bag (ovb). Figure 5 shows for the cure cycle MOD2 that there is a small lag between the temperatures of the two thermocouple positions at high cooling rates. The effects of temperature on the strain signal were corrected with the measurements inside the laminate when available.

3.2. Strain measurements

For conciseness, the focus in the following of this paper is on the strain data for the modified cure cycle MOD1, while the findings apply to all recorded data sets. On the left in Figure 6, the strain data for the MOD1 cure cycle is plotted over time for the two principal in-plane directions, where 0° indicates the fiber direction and rolling direction of the steel respectively, whereas 90° refers to the transverse direction. Significant differences between the two strain signals can be seen. While the transverse strain mostly follows the temperature profile, several distinct knees are identified in the strain signal in fiber direction despite a continuous temperature

curve. Furthermore, the residual strains at the end of the cure cycle show high positive values in the fiber direction and small negative values in the transverse direction. On the right in Figure 6 the strain in 0°-direction of the MOD1 cure cycle is compared to the strain of the MRCC. Here, a large difference in the residual strains is obvious at the end of the cure cycle, despite the temperatures being identical. The kink at the end of the MOD1 temperature curve originates from the opening of the door of the lab oven to allow the laminate to reach room temperature. In both the plots in Figure 6 shrinkage strains at the maximum process temperature of 180 °C can be recognized in all the strain curves. The strain data slightly decreases while the temperature remains constant. Although this behavior is visible in both the in-plane directions, it is more pronounced for the transverse direction where the cure shrinkage strains of the resin are not constrained by the high stiffness of the fibers.

Since more information is derived from the signal in 0°-direction and the residual stresses are one order of magnitude higher, the strains in that direction are mainly used for the interpretation of the results in the following. For the interpretation, it is advantageous to plot the strain data over the actual temperature. For the MOD1 cure cycle, this is shown in Figure 7. The strain signal is plotted over time with the distinction of the different stages in the modified cure cycle (compare to Figure 3) on the left. The plot on the right shows the same data plotted over the actual temperature during the manufacturing process. Before this characteristic curve is discussed in more detail in the next section 3.3, Figure 8 compares the strain data over temperature of the MOD1 cure cycle to the MRCC. Since no intermediate cooling takes place in the MRCC, the strain readings are relatively simple to interpret. While the strain increases with increasing temperature, its slope changes just before reaching the maximum temperature and decreases with a different slope during final cooling. The final residual strain is almost twice as big as in the modified cure cycle MOD1.
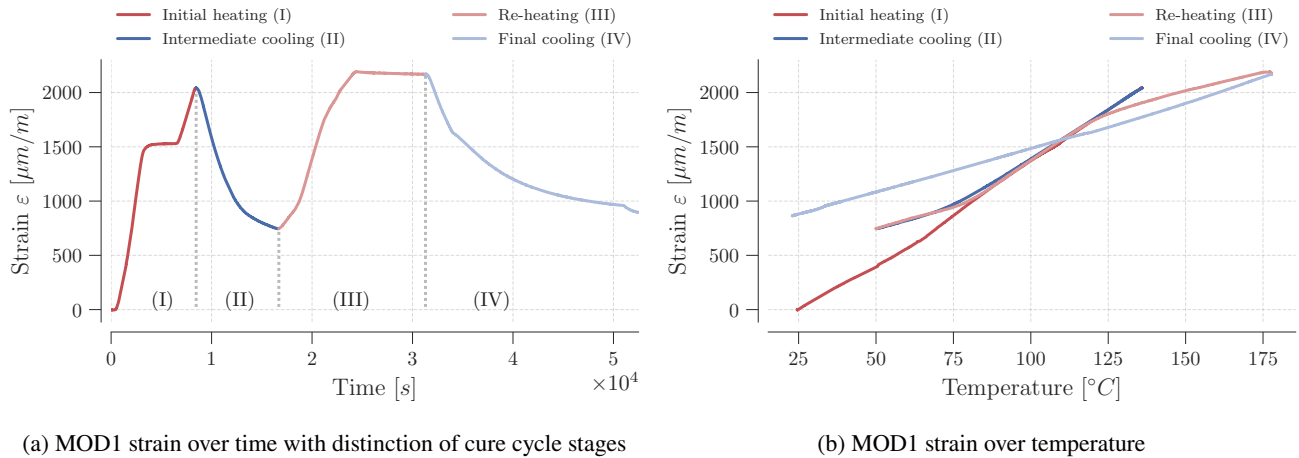
(a) MOD1 strain over time with distinction of cure cycle stages

(b) MOD1 strain over temperature

Figure 7: Strain data of MOD1 cure cycle with distinction of cure cycle stages as indicated in Figure 3 plotted over time (a) and temperature (b)
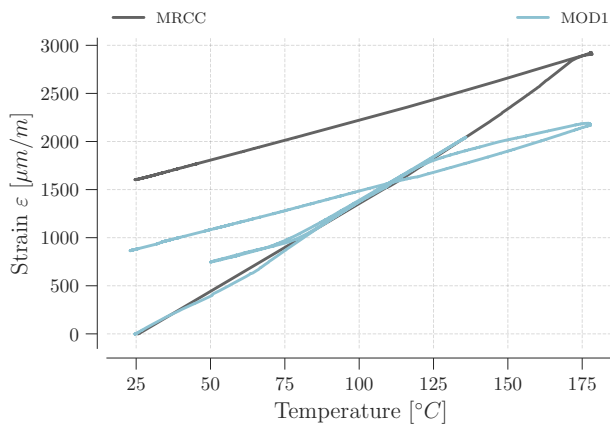

Figure 8: The comparison of the strain data of modified cure cycle MOD1 to the MRCC shows a significant reduction of residual strains.

3.3. Detailed strain data evaluation

In the strain gage data, not only the final residual strains can be examined but also distinct changes in the expansion behavior are identified. To interpret the data more easily, in Figure 9 the strain data for the MOD1 cure cycle as shown on the left in Figure 7 is separated into the different heating and cooling stages and plotted over the temperature. The slope of the curve is interpreted as the instantaneous coefficient of thermal expansion (CTE) of the substrate, the strain gage was applied to.

For high rate temperature changes, especially during the first heating ramp, some non-linearities are observed (see Figure 9 (a)). These are mainly due to temperatures deviations at the strain gage location and the location of the thermocouple. Since the strain signal is compensated for the temperature influence of the strain gage itself, slight deviations of the actual temperature at the strain gage location and the temperature measured will influence the strain signal. However, since the final residual strains are recorded

at the same temperature as the starting temperature of the measurement, this influence will not have an effect on the residual stress evaluation. Moreover, these effects cancel each other out in phases with a constant temperature. Additionally, consolidation effects in the laminate stack during the initial heating up to the dwell stage can also introduce non-linear behavior in the strain reading.

The section-wise linear CTE evaluation is a clear indicator of the resin state of cure. At the beginning of the cure cycle (a), the individual plies of the laminate behave independently of each other which is indicated by the CTE being in the range of the metal ply (18.79 ppm/K), that is in very good agreement with the CTE measured for the single material and shown in Table 3.

During the subsequent cool down (b), the CTE still is in the range of the independent metal. Only before dropping below a temperature of about 75 °C the CTE decreases significantly from 18.03 ppm/K to a value of 8.15 ppm/K, indicating a phase transition in the resin. This is attributed to the actual process temperature falling below the instantaneous glass transition temperature of the resin which is accompanied by the transition into its glassy elastic state.

After the subsequent re-heating (c) to the final cure temperature of 180 °C the CTE of the metal layer changes again from 7.94 ppm/K to 19.23 ppm/K at around the same process temperature. It is supposed that the resin transfers into its viscous state again which is accompanied by a loss of the interaction between metal and fiber plies and allows free thermal expansion of the metal. From this behavior it can be assumed that the degree of cure has not yet reached the gel point. Thus, any interlaminar forces that led to a change in the slope during the previous cooling step are released after passing T_g again. The final connection between the FML layers takes place at around 121 °C which again changes the slope to approximately the final CTE of the laminate (7.15 ppm/K). From there, it can be assumed that the degree of cure has passed the gel point and the laminate is not able to change into a viscous state again, despite a further increasing
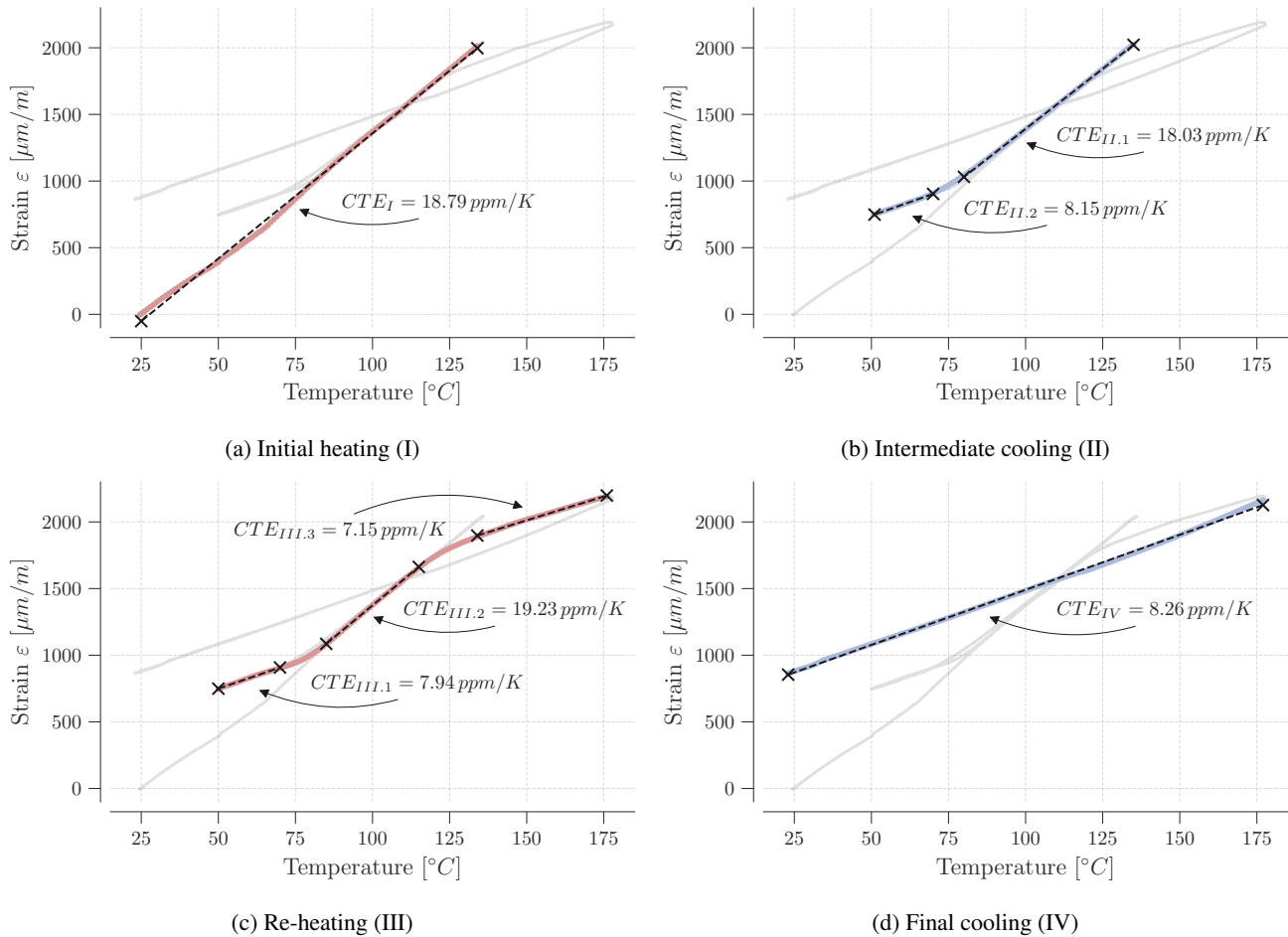
Figure 9: Linear CTE determination by section for the different phases during the smart cure cycle MOD1. The processing strains clearly show the phase changes of the matrix material from viscous to solid and vice versa. During the viscous state, the metal partner in the laminate is free to expand or contract with its own CTE. After gelation of the matrix, the laminate behaves like a homogeneous material.

process temperature. The slightly lower CTE values after gelation compared to the final CTE (8.26 ppm/K) can be attributed to the chemical shrinkage of the resin that takes place in parallel.

After the indissoluble bond between the individual layers of the FML has developed, the strain-temperature behavior is rather linear. The ultimate laminate CTE (8.26 ppm/K) during final cooling (d) is close to the calculated value in Table 3 (7.38 ppm/K). The slightly higher values in the fiber direction can be attributed to the different evaluation intervals. The CTE itself is not linearly dependent on temperature but increases with increasing temperature. Thus, the evaluation in between approx. 25 to 175 °C will produce slightly higher values than in between 55 to 95 °C as was used during the single ply CTE evaluation. Moreover, the values for the laminate in Table 3 were only calculated from the CTEs of the single materials whereby also the mechanical material properties are relevant which were taken from literature.

3.4. Determination of bonding temperature

The final bonding between the individual layers of the FML takes place at a certain temperature which can be derived from the strain measurements. The temperature is approximated by the highest change in the slope of the strain data. At this temperature, the transition from the thermally free expansion to the impeded expansion takes place.

To derive this temperature for all the cure cycles, the strain data during the heating to the final cure temperature is derived twice. Because of the noise in the strain data, the first derivative is smoothed before the second derivative is calculated. The temperature of the global minimum is defined as the bonding temperature. This is illustrated exemplarily in Figure 10 by the strain data of the MOD1 cure cycle.

The resulting bonding temperatures for each cure cycle and strain gage are given in Table 5. It is worth noting, that although the final residual strains slightly differ within the two strain gages applied to the same specimen, the bonding temperature is identical for all the strain gages used in the same experiment.
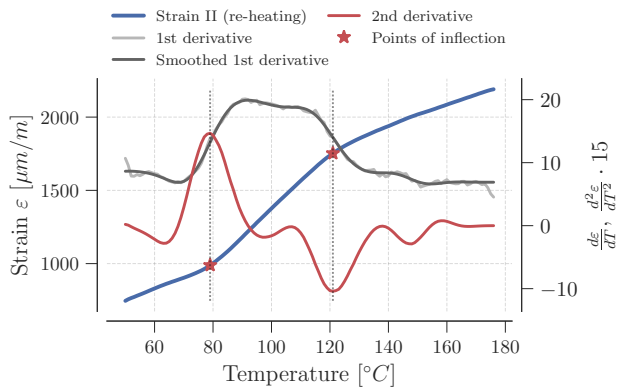
Figure 10: Evaluation of the bonding temperature by derivation of the strain data during re-heating (MOD1). The minimum of the second derivative shows the transition from free linear expansion to constraint linear expansion of the metal ply. Strain data only shows the second heating ramp, where the final bonding occurs.

Table 5
Bonding temperatures for each cure cycle and strain gage in this work

Cure cycle	SG1	SG2
MRCC	172 °C	-
MOD1	121 °C	121 °C
MOD2	129 °C	129 °C

Since this bonding temperature is easily determined with various measurement techniques, is is often assumed to be equal to the stress-free temperature and hence used to calculate the residual stress state in a laminate with Equation 2 [44]. The accuracy of this assumption, is discussed in the next section.

3.5. Residual stress determination

From the strain gage data during the final cooling step of the cure cycle, the residual stresses in the metal ply at any temperature are calculated with the classical laminate theory and Equation 3. For the residual stress comparison in this paper, the reference temperature is set to room temperature ($T_R = 20 \,°\text{C}$).

Since not all of the single strain measurements were cooled to 20 °C, the final cool-down step is linearly interpolated for all the strain gage data. From this interpolation, a final laminate CTE is derived for each measurement. The CTE values for each measurement are given in Table 6. The results show that the laminate CTE is independent of the cure cycle and is determined in the range of 8 to 8.8 ppm/K in the longitudinal direction and 23.2 to 24 ppm/K for the transverse direction. As explained earlier, this in good agreement with the calculated values from the CLT using the measured single ply CTEs as shown in Table 3.

The linear function for each curing cycle is complemented by the y-axis intercept b, which is also given in Table 6. Hence, the residual strains are calculated for all cure

cycles and the reference temperature. With these strains and Equation 3 the consequent residual stresses ($\sigma_{res, meas.}$) in the metal layer are calculated. Comparing the residual stresses in the longitudinal direction of the metal ply during the MRCC with the tensile strength of the metal material (Table 2) shows that the residual stresses already account for about 20 % of the material strength. By using smart cure cycles, the residual stress is reduced by around 50 % (compare MRCC to MOD1).

The measured absolute residual strains and consequent residual stresses in the metal ply can now be compared to estimated residual stress values using the determined bonding temperatures as the stress-free temperature for each cure cycle (see Section 3.4). Depending on the availability of data, either the single-ply CTEs and the calculated laminate CTEs as given in Table 3 or the measured laminate CTEs from the experiments can be used in the residual stress calculation. The results for the first approach (single-ply CTEs) are given as $\sigma_{res, calc.1}$ in Table 6. The values for the second approach, using the measured laminate CTEs, are given as $\sigma_{res, calc.2}$ in Table 6. The different values are calculated for each cure cycle with its respective bonding temperature and Equation 2:

$$T_{sf, calc.1} = T_{sf, calc.2} = T_{bonding} \qquad (4)$$

The values show significant differences between the two approaches and the measured residual stress levels. To visualize the differences, the respective residual stresses are plotted over the bonding temperature for each cure cycle and linearly interpolated in Figure 11. The Figure shows that assuming the bonding temperature to be equal to the stress-free temperature, results in a conservative estimation of the residual stress state for both calculation approaches. Moreover, the figure shows that the CTEs themselves have a large influence on the calculated residual stress levels. With the single-ply CTEs (Calc.1), the residual stresses are significantly overestimated for the laminate in this work. Using the mean of the measured laminate CTEs (Calc.2) from Table 6 continues to be a conservative approach by slightly overestimating the residual stresses. The difference between the two calculation approaches clearly shows the relevance of a correct CTE determination.

The comparison between measured and calculated values implies that for a more accurate representation of the residual stresses, the stress-free temperature can be assumed to be lower. By reducing the stress-free temperature in the second calculation approach by $-11 \,\text{K}$ it is ensured that the residual stress levels are not underestimated for either of the cure cycles. Thus, the MRCC is set as the reference to determine the correction factor.

$$T_{sf, calc.2, corrected} = T_{bonding} - 11 \,\text{K} \qquad (5)$$

The corrected calculation is plotted with the dashed line in grey color in Figure 11. This correction factor can also be explained by the measured strain data. It accounts for the strains due to cure shrinkage effects that take place after

Table 6
Residual strains for different cure cycles in this work and corresponding linear equation in the form of $\varepsilon_{res} = CTE \cdot T_R + b$ and consequent residual stresses calculated with Equation 3 for the reference temperature $T_R = 20\,°C$. Calculated residual stresses (calc. 1 and calc. 2) were derived from the bonding temperatures ($T_{sf} = T_{bonding}$) and Equation 2 for $T_R = 20\,°C$ as well.

Cure cycle (SG 1/2)	CTE [ppm/K]	y-intercept 'b' [μm/m]	ε_{res} [μm/m]	$\sigma_{res,meas.}$ [MPa]	$T_{bonding}$ [°C]	$\sigma_{res,calc.1}$ [MPa]	$\sigma_{res,calc.2}$ [MPa]
MRCC-SG1 (0°)	8.09	(-)[a]	-	-	-	-	-
MRCC-SG2 (0°)	8.57	1372.90	1544	257	172	306	278
MOD1-SG1 (0°)	8.26	664.25	829	123	121	203	185
MOD1-SG2 (0°)	8.51	750.26	920	141	121	203	185
MOD2-SG1 (0°)	8.78	912.64	1088	174	129	219	199
MOD2-SG2 (0°)	8.02	903.76	1064	169	129	219	199
Mean	8.37						
MRCC (90°)	23.23	-1250.40	-786	-63	-	-36	-38
MOD1 (90°)	23.98	-1162.08	-682	-85 / -80	-	-24	-25
MOD2 (90°)	-	-	(-682)[b]	-70 / -71	-	-26	-27
Mean	23.61						

[a] not meaningful due to jumps of the signal, [b] from MOD1 90, due to malfunction of SG
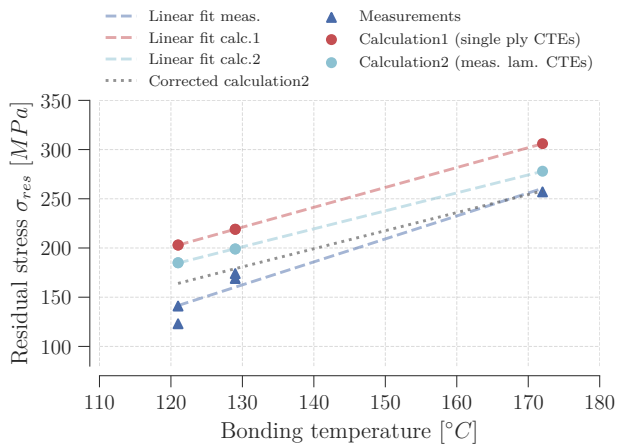

Figure 11: Assuming the bonding temperature to be equal with the stress-free temperature, overestimates the final residual stresses in 0°-direction of the metal layer for both calculation approaches.

the final bonding of the plies and can be interpreted as the vertical shift of the strain curves after bonding and final cooling (see Figure 9). The influence of this effect is greater for the MOD cure cycles compared to the MRCC, where the final bonding takes place just before the maximum process temperature.

3.6. Comparison of SG to FBG measurement

During the MOD2 cure cycle, an FBG sensor was additionally embedded into the middle of the CFRP stack below the top metal layer. The FBG signal was recorded in parallel to the strain gage signal. As stated in the beginning, the FBG measurements can not directly be used to quantify the residual stress state. However, the same laminate behavior during the re-heating stage and the final cooling of the

modified cure cycle is observed in the FBG data. Figure 12 shows the strain gage data during the cure cycle stages III and IV on the left. Again, the re-heating is shown in red color, whereas the final cooling is plotted in blue color. On the right in Figure 12, the corresponding FBG data is plotted. It is given as the wavelength shift due to the combination of a strain and a temperature-dependent change in the refractive index of the Bragg grating.

In both the plots, the transition from below the glass transition temperature to a renewed independent expansion state and the point of final bonding of the individual layers can be identified. In contrast to the strain gage data, the FBG signal transitions into a thermal expansion behavior with a smaller gradient at 77\,°C. At this temperature, the resin transitions into its viscous state, which is accompanied by a loss of the connection between FBG and fiber ply as well as between the different FML layers. Hence the thermal expansion behavior of the sensor and the fiber ply is dominant, with both of them being smaller compared to the metal. Moreover, the FBG data shows a non-linear sensor behavior during the following stage which is attributed to the interference of temperature-induced elongation of the sensor and the fiber ply and cure shrinkage strains caused by the resin. Only at 130\,°C the gradient is increasing again to almost the same value as during the final cool-down, which indicates laminate behavior from this point onwards with the single FML plies bonded together.

A small deviation in the evaluation of the prominent temperatures by calculating the second derivative exists. However, the temperature of the final connection deviates only by 2\,K from each other. This deviation is considered relatively small, given that two different measuring systems with different sensors in two different layers of the FML were used for the data collection.
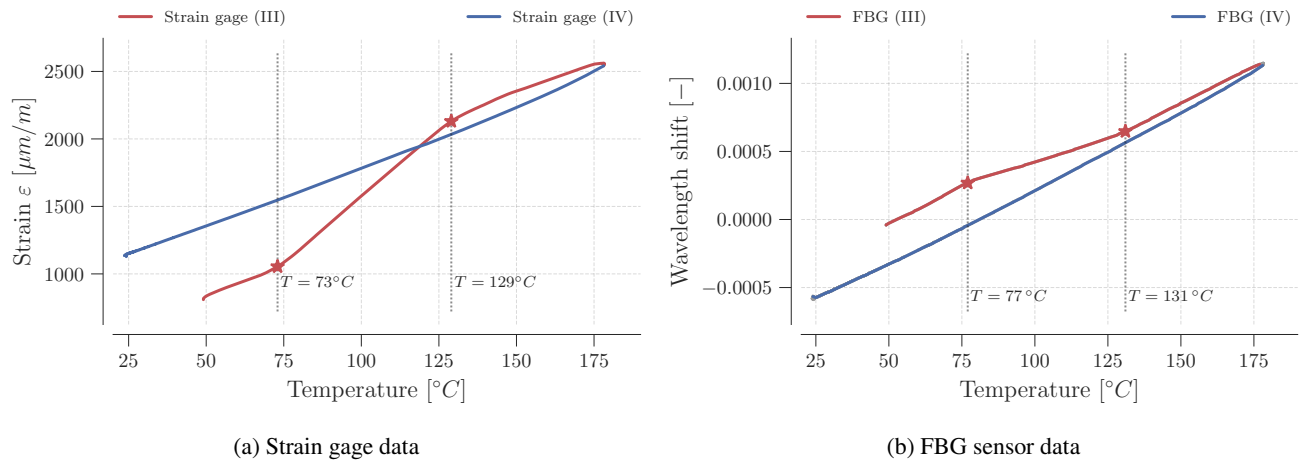
Figure 12: Comparison of strain data for the MOD2 cure cycle during re-heating (III) and final cooling (IV) with the strain gage applied to the metal layer and the FBG embedded into the fiber layer

4. Discussion

The strain gage approach presented earlier and applied in this work is a measurement technique that is very suitable to monitor the curing strains over an entire cure cycle of fiber metal laminates. With this technique, absolute residual strains in an FML laminate can be measured with the strain state before the start of the manufacturing process serving as the baseline. This is a big advantage over e.g. FBG sensors where the strain information between the start of the cure cycle and the point of bonding between the individual layers is not evaluable. Hence significant points in the strain signal need to be used as a tool for the residual stress calculation. One of these points is the temperature at which the single layers of the laminate bond together which is easily identified by a significant change in the gradient of the strain signal. The results show, that by setting the bonding temperature equal to the stress-free temperature, a conservative estimation of the residual stress state can be calculated. Furthermore, the CTEs themselves as the basis for the calculation have a large influence on the approximated residual stress state using the stress-free temperature approach. With the material CTEs known, a correction factor can be introduced accounting for the cure shrinkage strains. This promotes a second point in the strain data to be used as a stress-free temperature, which is the intersection of the strain curve during re-heating and final cooling (see Figure 9). This point is likewise easily determined in the strain data of the modified cure cycles and the respective temperature is below the bonding temperature, such that the cure shrinkage strains are accounted for. However, for the MRCC this point is not as pronounced. Thus, this approach needs greater attention in future investigations.

In terms of smart cure cycle optimization, two consequences can be derived from the results in this work. It can be assumed that the minimum temperature during the intermediate cooling step does not need to fall below the glass transition temperature, as the curing reaction will be slowed down significantly. This assumption is supported by the fact that the transition during cool down takes place almost at the same temperature as during the subsequent re-heating stage. Hence, the glass transition temperature did not change significantly which indicates no further progress in the curing reaction. As a consequence, the smart cure cycle as proposed by [19] can be further modified by halting the cooling step as soon as a temperature of around 80 °C is reached. Thus, the curing reaction can further proceed and the bonding temperature possibly even shifted to a lower value. For research applications, this could be complemented by a very slow re-heating rate, such that the glass transition temperature continuously is above the actual process temperature. However, whether this is a valid assumption needs to be further investigated by additional experiments.

Another consequence for industrial applications can be drawn where a post-curing step of a laminate is preferably realized in an oven instead of an autoclave with a lot higher operational costs. For all the modified cure cycles in this work, this is not possible since the laminate transfers into the viscous state during re-heating. This in general is accompanied by a loss of the dimensional stability of a laminate. Thus, for this type of cure cycle optimization, it needs to be ensured, that the gel point has been reached before transferring a composite part into an oven. With the strain gage technique, the cure cycle can be optimized such that no softening of the material takes place upon re-heating.

Comparing the differences in the residual stress states between the modified cure cycles in this work with the manufacturer recommended cure cycle, reductions of the stress level by around 50 % could be achieved, which is an increase compared to the literature (e.g. [19]). For research applications where the influence of the residual stress state on other parameters shall be investigated, the question arises, whether the residual stress level can even be increased compared to the MRCC. Based on the results in this work it is assumed that by increasing the heating rate during the heating ramp to the final cure temperature of the MRCC,

the bonding temperature of 172 °C may be shifted close to 180 °C and consequently the residual stress level is further increased. An even higher bonding temperature might be achieved by initially overshooting the final cure temperature during a fast heating ramp. Again these assumption need to be further supported by experiments.

The results in this work showed some differences in the strain signal of two strain gages applied to the same specimen (see MOD1 and MOD2 in Table 6). It needs to be further investigated whether there are inhomogeneities in the residual stress level of a laminate or the differences originate from the measurement set up or imperfections in the strain gage application.

The combined experiment with strain gages and an FBG sensor validates the finding, that the phase transitions of the resin and the interaction between metal and fiber plies in the FML can be accurately determined by only applying strain gages to the metal layer.

5. Conclusion and outlook

In this work it was shown, that strain gages bonded to the metal layer of an FML are an easy and accurate method to measure the curing strains induced during manufacturing. As the metal behaves purely thermo-elastic during the manufacturing process, absolute strains can be determined and residual stresses directly calculated.

With the cure cycles used in this work, the residual stress level of the CFRP-steel laminate could be reduced by around 50 %. Further conclusions for modified curing cycles are drawn from the interpretation of the recorded strain data. The minimum temperature after intermediate cooling can possibly be moved to higher values. Combined with slower re-heating rates, the residual stress state can potentially be even further reduced. Thus the strain gage technique seems promising not only for residual stress determination but also for cure cycle optimization.

Furthermore, it was shown for the CFRP-steel laminate in this work, that assuming the stress-free temperature to be equal with the bonding temperature gives a conservative estimation of the residual stress state. The stress-free temperature can be lowered by a correction factor resulting in more accurate residual stress levels. The correction factor in this work was determined to be -11 K. The main reason for this is, that the assumption does not consider the curing related shrinkage strains of the resin. However, the correction requires a comprehensive knowledge of the coefficients of thermal expansion of the single materials as well as the final laminate to ensure that the residual stresses are not underestimated by the correction.

It needs to be further investigated, whether the strain gages can also be applied to a metal layer inside an FML laminate. Thus, a gradient in the residual stress state over the thickness of a laminate can be determined.

The convenience and ease of handling of the strain gage technique promote the presented experimental setup to be used for pure composite materials as well. Although residual stresses can only be measured in FMLs the approach may be adapted such that the resin characteristics can be analyzed. An instrumented metal layer or strain gages attached to a small metal plate can be integrated into or put on top of a composite laminate. Thus, similar to the FBG technique, the resin behavior can be analyzed, the material characterized and implications for cure cycles be drawn.

The authors recommend to complement the present work with additional studies focusing on the effects of autoclave processing, layup variation combined with the indicated strategy for cure-cycle modification.

Acknowledgment

CRediT authorship contribution statement

Johannes Wiedemann: Conceptualization, Methodology, Investigation, Data Curation, Writing - Original Draft, Writing - Review and Editing, Visualization. **Robert Prussak:** Methodology, Resources, Writing - Review and Editing. **Erik Kappel:** Methodology, Writing - Review and Editing. **Christian Hühne:** Conceptualization, Writing - Review and Editing, Funding acquisition, Project administration.

Data availability

The raw/processed data required to reproduce these findings cannot be shared at this time as the data also forms part of an ongoing study.

References

[1] M. Abouhamzeh, Distortions and Residual Stresses of GLARE Induced by Manufacturing, Ph.D. thesis, Delft University of Technology, 2016. doi:10.4233/uuid:1f1b3e5c-72b8-440c-8d98-4b4c82814fb6.

[2] G. Gardiner, The resurgence of GLARE: Airbus pursues fiber metal laminates for future narrowbody construction, citing cost, weight, repair and lightning strike benefits., 2016. URL: https://www.compositesworld.com/articles/the-resurgence-of-glare.

[3] D. Stefaniak, Improving residual strength of unidirectionally reinforced plastic laminates by metal layering, Dissertation, Technische Universität Carola-Wilhelmina zu Braunschweig, 2017.

[4] B. Kolesnikov, A. Fink, C. Hühne, D. Stefaniak, H. Borgwardt, Strukturelement aus einem Hybridlaminat, 2010. URL: https://patents.google.com/patent/DE102010035324A1/de.

[5] D. Stefaniak, B. Kolesnikov, E. Kappel, C. Hühne, Improving Impact Endangered CFRP Structures by Metal-Hybridisation, in: 12th European Conference on Spacecraft Structures, Materials and Environmental Testing, volume 691 of *ESA Special Publication*, 2012, p. 57.

[6] A. Pototzky, D. Stefaniak, C. Hühne, Potentials of load carrying conductor tracks in new vehicle structures, in: K. Dröder, T. Vietor (Eds.), Technologies for economical and functional lightweight design, Zukunftstechnologien für den multifunktionalen Leichtbau, Springer Berlin Heidelberg, Berlin, Heidelberg, 2019, pp. 79–90. URL: https://doi.org/10.1007/978-3-662-58206-0_8.

[7] C. Hühne, C. Ückert, O. Steffen, Multifunktionale Flügelvorderkante in Multimaterialbauweise, Lightweight Design 9 (2016) 28–33. doi:10.1007/s35725-015-0065-6.

[8] I. Roese-Koerner, J. Bachmann, F. Martaus, G. Mirra, J. M. Liebisch, P. Lorsch, Improving material solutions to mitigate fire, smoke and fumes in cabin environment: Final report - FUTURE SKY Safety, 2018. URL: https://www.futuresky-safety.eu/wp-content/uploads/2018/07/FSS_P7_DLR_D7.13_v2.0.pdf.

[9] Y. Boose, E. Kappel, D. Stefaniak, R. Prussak, A. Pototzky, L. Weiß, Phenomenological investigation on crash characteristics of thin layered CFRP-steel laminates, International Journal of Crashworthiness 182 (2020) 1–10. doi:10.1080/13588265.2020.1787681.

[10] A. Fink, P. P. Camanho, J. M. Andrés, E. Pfeiffer, A. Obst, Hybrid CFRP/titanium bolted joints: Performance assessment and application to a spacecraft payload adaptor, Composites Science and Technology 70 (2010) 305–317. doi:10.1016/j.compscitech.2009.11.002.

[11] J. C. Both, Tragfähigkeit von CFK-Metall-Laminaten unter mechanischer und thermischer Belastung: Zugl.: München, Techn. Univ., Diss., 2014, Ingenieurwissenschaften, Dr. Hut, München, 2014. URL: http://mediatum.ub.tum.de/node?id=1173300.

[12] E. Petersen, D. Stefaniak, C. Hühne, Experimental investigation of load carrying mechanisms and failure phenomena in the transition zone of locally metal reinforced joining areas, Composite Structures 182 (2017) 79–90. doi:10.1016/j.compstruct.2017.09.002.

[13] A. Fink, Lokale Metallhybridisierung zur Effizienzsteigerung von Hochlastfügestellen in Faserverbundwerkstoffen, Dissertation, Technische Universität Carolo-Wilhelmina zu Braunschweig, Braunschweig, 2010.

[14] D. Düring, L. Weiß, D. Stefaniak, N. Jordan, C. Hühne, Low-velocity impact response of composite laminates with steel and elastomer protective layer, Composite Structures 134 (2015) 18–26. doi:10.1016/j.compstruct.2015.08.001.

[15] D. Düring, E. Petersen, D. Stefaniak, C. Hühne, Damage resistance and low-velocity impact behaviour of hybrid composite laminates with multiple thin steel and elastomer layers, Composite Structures 238 (2020) 111851. doi:10.1016/j.compstruct.2019.111851.

[16] H. Sohn, Effects of environmental and operational variability on structural health monitoring, Philosophical transactions. Series A, Mathematical, physical, and engineering sciences 365 (2007) 539–560. doi:10.1098/rsta.2006.1935.

[17] N. Zobeiry, A. Poursartip, The origins of residual stress and its evaluation in composite materials, in: P. W. R. Beaumont (Ed.), Structural integrity and durability of advanced composites, Woodhead publishing series in composites science and engineering, Elsevier, Amsterdam, 2015, pp. 43–72. doi:10.1016/B978-0-08-100137-0.00003-1.

[18] R. Prussak, D. Stefaniak, C. Hühne, M. Sinapius, Evaluation of residual stress development in FRP-metal hybrids using fiber Bragg grating sensors, Production Engineering 12 (2018) 259–267. doi:10.1007/s11740-018-0793-4.

[19] R. Prussak, D. Stefaniak, E. Kappel, C. Hühne, M. Sinapius, Smart cure cycles for fiber metal laminates using embedded fiber Bragg grating sensors, Composite Structures 213 (2019) 252–260. doi:10.1016/j.compstruct.2019.01.079.

[20] H. S. Kim, S. W. Park, D. G. Lee, Smart cure cycle with cooling and reheating for co-cure bonded steel/carbon epoxy composite hybrid structures for reducing thermal residual stress, Composites Part A: Applied Science and Manufacturing 37 (2006) 1708–1721. doi:10.1016/j.compositesa.2005.09.015.

[21] National Institute for Aviation Research - Wichita State University, Hexcel 8552 AS4 Unidirectional Prepreg at 190 gsm & 35% RC Qualification Material Property Data Report, 2011. URL: https://www.wichita.edu/research/NIAR/Research/hexcel-8552/AS4-Unitape-2.pdf.

[22] Stahl-Becker GmbH, Datenblatt: Nicht rostender Federbandstahl (1.4310): Technical Data Sheet, 2022. URL: https://www.stahlbecker.de/umbracopdfgenerator/1884.pdf.

[23] Hexcel Corporation, Product data sheet HexPly 8552, 2020. URL: https://www.hexcel.com/user_area/content_media/raw/HexPly_8552_eu_DataSheet.pdf.

[24] E. Kappel, A zone-based approach to predict process-induced distortions of composite structures based on a 'spring-in reference curve', Composite Structures 209 (2019) 143–149. doi:10.1016/j.compstruct.2018.10.045.

[25] Tokyo Measuring Instruments Laboratory Co., Ltd., Strain Gauge Adhesives, 2021. URL: https://tml.jp/eng/documents/strain_gauge/adhesive_list.pdf.

[26] A. T. Nettles, Basic Mechanics of Laminated composite plates, 1994. URL: https://ntrs.nasa.gov/citations/19950009349.

[27] E. Kappel, R. Prussak, On abnormal thermal-expansion properties of more orthotropic M21E/IMA carbon-fiber-epoxy laminates, Composites Communications 17 (2020) 129–133. doi:10.1016/j.coco.2019.11.014.

[28] H. Schürmann, Konstruieren mit Faser-Kunststoff-Verbunden, Springer Berlin Heidelberg, Berlin, Heidelberg, 2007. doi:10.1007/978-3-540-72190-1.

[29] A. A. Johnston, An integrated model of the development of process-induced deformation in autoclave processing of composite structures, Dissertation, University of British Columbia, Vancouver, Kanada, 1997. doi:10.14288/1.0088805.

[30] K. Y. Blohowiak, J. H. Osborne, K. A. Krienke, Surface pretreatment of metals to activate the surface for sol-gel coating, 1999. URL: https://patents.google.com/patent/US5869140A/en.

[31] 3M Aerospace and Commercial Transportation Division, 3M™ Surface Pre-Treatment AC-130-2, 2015. URL: https://multimedia.3m.com/mws/media/1063834O/3m-surface-pre-treatment-ac-130-2-application-guide.pdf.

[32] S. R. White, H. T. Hahn, Cure Cycle Optimization for the Reduction of Processing-Induced Residual Stresses in Composite Materials, Journal of Composite Materials 27 (1993) 1352–1378. doi:10.1177/002199839302701402.

[33] S. S. Kim, H. Murayama, K. Kageyama, K. Uzawa, M. Kanai, Study on the curing process for carbon/epoxy composites to reduce thermal residual stress, Composites Part A: Applied Science and Manufacturing 43 (2012) 1197–1202. doi:10.1016/j.compositesa.2012.02.023.

[34] R. Prussak, D. Stefaniak, C. Hühne, M. Sinapius, Residual Stresses in Intrinsic UD-CFRP-Steel-Laminates - Experimental Determination, Identification of Sources, Effects and Modification Approaches, in: 20th Symposium on Composites, Materials Science Forum, Trans Tech Pubn, 2015, pp. 369–376. URL: https://www.scientific.net/MSF.825-826.369.pdf. doi:10.4028/www.scientific.net/MSF.825-826.369.

[35] N. J. Pagano, H. T. Hahn, Evaluation of Composite Curing Stresses, in: G. M. L. Gladwell, J. N. Reddy (Eds.), Mechanics of Composite Materials, volume 34 of Solid mechanics and its applications, Springer Netherlands, Dordrecht, 1994, pp. 57–69. URL: https://doi.org/10.1007/978-94-017-2233-9_6.

[36] A. S. Crasto, R. Y. Kim, On the Determination of Residual Stresses in Fiber-Reinforced Thermoset Composites, Journal of Reinforced Plastics and Composites 12 (1993) 545–558. doi:10.1177/073168449301200505.

[37] L. P. Canal, M. Benavente, M. Hausmann, V. Michaud, Process-induced strains in RTM processing of polyurethane/carbon composites, Composites Part A: Applied Science and Manufacturing 78 (2015) 264–273. doi:10.1016/j.compositesa.2015.08.018.

[38] C. M. Lawrence, D. V. Nelson, J. R. Spingarn, T. E. Bennett, Measurement of process-induced strains in composte materials using embedded fiber optic sensors, 1996. doi:10.2172/226060.

[39] A. S. Crasto, R. Y. Kim, J. D. Russell, In situ monitoring of residual strain development during composite cure, Polymer Composites 23 (2002) 454–463. doi:10.1002/pc.10447.

[40] Y. K. Kim, I. M. Daniel, Cure Cycle Effect on Composite Structures Manufactured by Resin Transfer Molding, Journal of Composite Materials 36 (2002) 1725–1743. doi:10.1177/0021998302036014598.

[41] M. R. Wisnom, M. Gigliotti, N. Ersoy, M. Campbell, K. D. Potter, Mechanisms generating residual stresses and distortion during manufacture of polymer–matrix composite structures, Composites Part A: Applied Science and Manufacturing 37 (2006) 522–529. doi:10.1016/j.compositesa.2005.05.019.

[42] G. Twigg, A. Poursartip, G. Fernlund, An experimental method for quantifying tool–part shear interaction during composites processing, Composites Science and Technology 63 (2003) 1985–2002. doi:10.1016/S0266-3538(03)00172-6.

[43] E. Kappel, R. Prussak, J. Wiedemann, On a simultaneous use of fiber-Bragg-gratings and strain-gages to determine the stress-free temperature Tsf during GLARE manufacturing, Composite Structures 227 (2019). doi:10.1016/j.compstruct.2019.111279.

[44] E. Kappel, On thermal-expansion properties of more-orthotropic prepreg laminates with and without interleaf layers, Composites Part C: Open Access 3 (2020) 100059. doi:10.1016/j.jcomc.2020.100059.